Earth Planets Space, **51**, 897–906, 1999

Seasonal variations of gravity wave structures in OH airglow with a CCD imager at Shigaraki

T. Nakamura, A. Higashikawa, T. Tsuda, and Y. Matsushita

Radio Atmospheric Science Center, Kyoto University, Uji, Kyoto 611-0011, Japan

(Received August 17, 1998; Revised April 26, 1999; Accepted May 11, 1999)

A wideview CCD imager for OH airglow observations was operated at the MU radar site in Shigaraki, Japan (35°N, 136°E). From the 18 months' observation, dominant gravity wave components in the OH images are extracted, and seasonal variation of the characteristics of the waves is investigated. These waves typically have short horizontal wavelengths (5 km–60 km) and short periods (5 min–30 min), with horizontal phase speeds of 0–100 m/s. All the wave events are separated into two groups by a boundary of a horizontal wavelength of 17.5 km, which is close to the boundary between ripples and bands. For the waves with larger horizontal wavelengths, the horizontal propagation direction showed clear seasonal variation with summer eastward and winter westward preferences, with a change of direction in mid-March and at the end of September. This suggests that these waves are propagated from the lower atmosphere and filtered in the middle atmosphere by the mean winds. However, the small scale waves propagate in almost all azimuths with a slight seasonal variation. Therefore, *in-situ* generation would be the major source of such waves although the wavelength as a physical boundary between the two groups could be smaller than 17.5 km. The seasonal variation of the wave parameters especially between summer/winter and equinoctial months is also discussed. The waves with small horizontal wavelengths ($<$15 km), longer periods ($>$10 min), and slow horizontal phase speeds ($<$30 m/s) are mainly seen in summer/winter.

1. Introduction

It is now understood that in the middle atmosphere gravity waves play an important role in transporting energy and momentum from the lower atmosphere, which determines the general circulation, and the temperature structure of the mesosphere and lower thermosphere. Also, a significant proportion of the gravity waves are thought to propagate into the upper atmosphere, which causes the input of momentum and energy in the thermosphere. There are various observational techniques for the gravity waves in the upper middle atmosphere, such as radar, lidar, and satellite measurements. However, each of these techniques has its own system limitation for gravity wave observations and can only be used to observe a proportion of the gravity wave components in the widely spread frequency and wavenumber spectrum. Therefore, a combination of observational methods is very important for studying the whole characteristics of the gravity waves (Gardner and Taylor, 1998).

Among the above mentioned observational techniques, radar observations have contributed quite a bit to gravity wave studies in the mesosphere and lower thermosphere. In radar observations, the wave components are mainly analyzed in time series of radial or horizontal wind velocities. Gravity wave energy, and its seasonal, height and latitudinal variations have been studied by many authors (e.g., Tsuda *et al.*, 1994). A few radars such as the middle and upper atmosphere radar (MU radar) have clarified the momentum flux associated with the gravity waves and the mean wind accelerations in the mesosphere have been deduced (Tsuda *et al.*, 1990, Nakamura *et al.*, 1993a). Attempts to clarify the horizontal scale or structure of these gravity waves based on radar observations have also been reported despite the difficulties. The MU radar provided the parameters of the gravity waves in the vertical profile of wind velocities and its seasonal variation. The dominant components were inertia gravity waves with fairly large horizontal wavelengths ($\sim$1,000 km) (Nakamura *et al.*, 1993b). The GRAVMET system, which is a set of MF radars located about 50 km apart, also clarified the horizontal structure, for fairly large scale gravity waves (Manson and Meek, 1988).

On the other hand, imaging observations of airglow around the mesopause region are suitable for investigating the horizontal structure of gravity waves more directly and clearly, and have been applied to observe the characteristics of gravity waves with short periods ($<$1 hour) and small horizontal wavelengths (5 $\sim$ 100 km) at various locations, although only the waves with long vertical wavelengths are observed because of the thickness of the airglow layer ($\sim$10 km). These observations are mainly carried out on a campaign basis (e.g., Peterson, 1979; Clairemidi *et al.*, 1985; Taylor *et al.*, 1987). In some cases, the source of these waves was thought to be in the troposphere, from which the gravity waves propagate upward in the middle atmosphere (Taylor and Hapgood, 1988). However, *in-situ* excitation at airglow altitudes or ducting in the upper middle atmosphere has also been suggested by observations and numerical modelings (Fritts *et al.*, 1993; Isler *et al.*, 1997).

Copy right© The Society of Geomagnetism and Earth, Planetary and Space Sciences (SGEPSS); The Seismological Society of Japan; The Volcanological Society of Japan; The Geodetic Society of Japan; The Japanese Society for Planetary Sciences.

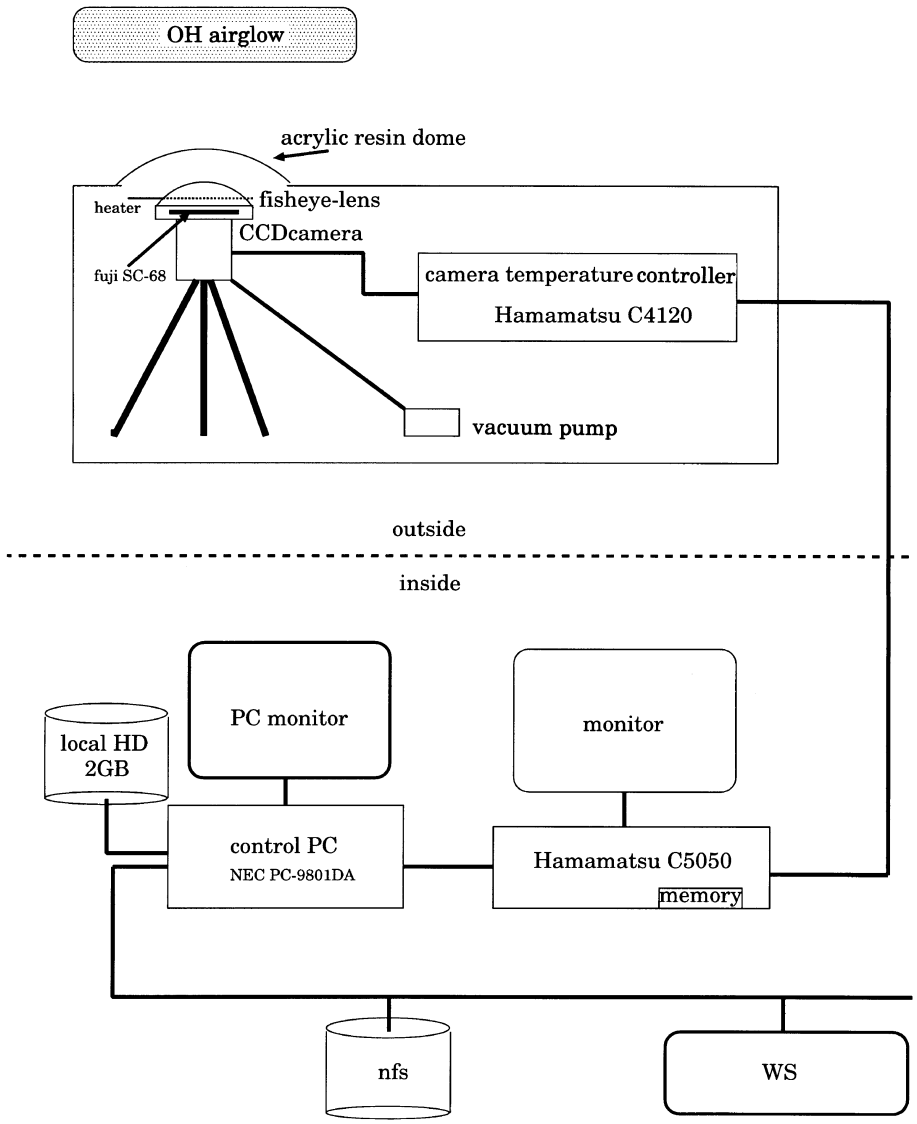

Fig. 1. Systematic diagram of the OH CCD imager used in this study.

The recent development of the CCD (Charge Coupled Device) camera has enabled us to carry out airglow imaging with better sensitivity and observations have been carried out at various locations (e.g., Taylor *et al.*, 1995). Cooperative observation with other instruments such as a sodium lidar or a radar has been applied to clarify evidence of a small scale wave pattern generated by the convective instability due to a larger scale gravity wave (Fritts *et al.*, 1997; Hecht *et al.*, 1997). However, long-term observations at a fixed location, which can investigate the annual variations of the horizontal structure of gravity waves in the mesopause region, have not been reported yet although some work revealed a part of seasonal variation (Wu and Killeen, 1996). A wideview CCD imager for OH airglow observations was installed at the MU radar observatory in Shigaraki (34°N, 136°E), Japan, and has been operated automatically. In this paper, we present an overview of the observations from November 1996 to May 1998, and describe the characteristics of the observed (or ground-based) parameters of the dominant gravity wave components seen in the OH images. The detailed analyses including measurement of intrinsic wave parameters of the waves derived using the background wind field measured by the MU radar and characteristics of the vertical propagation will be discussed elsewhere, and thus are not covered in this paper.

2. Observations

2.1 CCD imager setup

The CCD imager used here is a simple wideview camera with a cooled CCD chip and broadband infrared filter. Figure 1 shows the system setup of the imager. The primary lens is a fish-eye type one (Fisheye Nikkor, 8mm/F2.8), the lens being equipped with a tri-acetyl cellulose infrared filter (Fuji: SC-68). The image is focused on the CCD chip, with dimensions of 12 mm × 12 mm (TI TC-215), in the cooled CCD camera, Hamamatsu C-3640. The size of CCD chip limits the field of view to 93.9° × 93.9° in the NS and EW directions, and 132.8° in the diagonal direction. The total filter pass band is approximately 680–1000 nm, including the sensitivity of the CCD chip. It should be noted that in

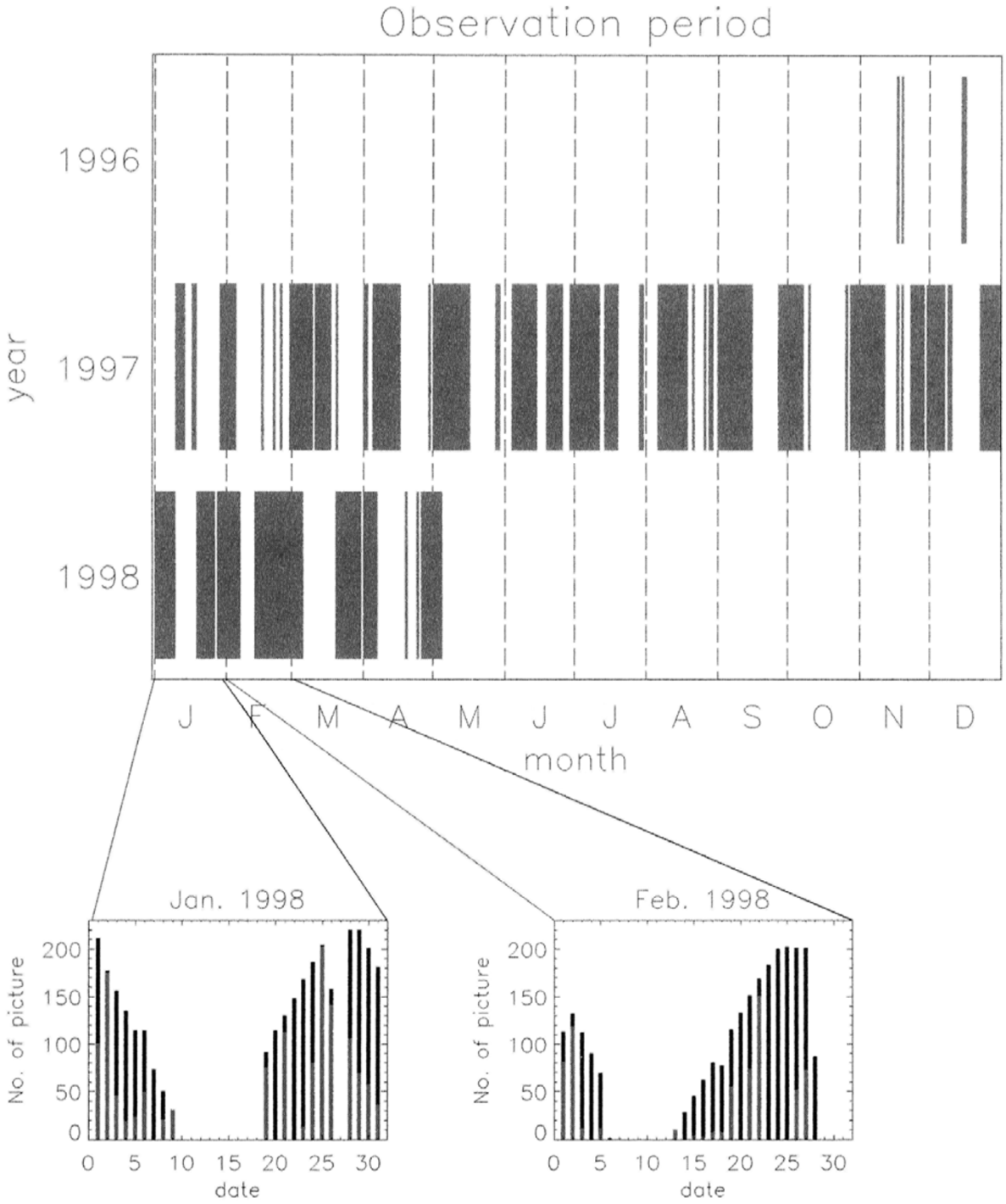

Fig. 2. The observation period of the OH CCD imager at Shigaraki used in this study. The bottom panels show the numbers of images on individual nights in January and February, 1998. The light and dark shading shows clear and cloudy (or rainy) images, respectively.

this pass band, emission of the O_2 (0, 1) atmospheric band as well as continuum nightglow could be detected. The wave-like structure in the O_2 atmospheric band image has often been reported in previous papers. However, simultaneous observations at the same location using multicolor CCD imagers, OMTI (Optical Mesosphere Thermosphere Imagers (Shiokawa *et al.*, 1999)) in January–March 1998 during the PSMOS campaign in Japan suggested that the contamination by O_2 airglow is less than 10%, and therefore no significant interference by the gravity wave pattern seen in the O_2 atmospheric band is expected. The image data obtained with the CCD chip are transferred to signal processing unit (C5050), where the dark current image taken every 90 minutes is subtracted. The images are then transferred to a PC (NEC: 9801DA) through a GP-IB interface and stored on a harddisk. The PC is connected to a local network through Ethernet. Control software on the PC automatically operates the imager system, but detailed parameters of observations such as the start and end times can be changed remotely by editing the parameter file on the network.

The exposure time was set at 100–120 sec, and because of the transfer time to the PC the interval between the images was set at 3 minutes. The shortest period of gravity waves is limited by the Brunt Väisälä frequency, i.e., around 5 minutes at the altitude of OH airglow layer (∼87 km), which corresponds to the Nyquist period of 2.5 minutes. A Doppler shift due to the background mean wind may make the Nyquist period required even smaller. However, because of spatial non-uniformities in the waveform of modulation of the airglow layer due to the gravity waves, we can determine the parameters of gravity waves with periods of less than 6 minutes without ambiguity due to the aliasing effect in most cases (Taylor *et al.*, 1997).

The outside equipment shown in Fig. 1 is enclosed in a box with an acrylic dome above the top of the primary lens, to allow automatic operation under various weather conditions. Figure 2 shows the observation period for the OH images obtained with the CCD imager used in this study, with the details of the numbers of images obtained on each night shown for January and February 1998, as an example. The observation started in November 1995 on a campaign basis, with manual operation of the system without the enclosure of the camera in a box. On January 29, 1997, the camera system was placed in a box and automatic operation started. Basically, the imager has been operated for 2–3 weeks around the new moon each month. However, occasionally the system was not operated during a totally cloudy night or was stopped because of a malfunction. The imager has been basically operated under the conditions that the moon is below the horizon and the solar zenith angle is greater than 105 degrees, which causes a monthly variation of the numbers of image obtained each night, as can be seen in the bottom panel in Fig. 2. In total, we obtained images without clouds on 161 nights between November 1996 and May 1998. Between May and July in 1997, the imager sometimes stopped due to malfunction caused by the high temperature in the daytime as well as the bad weather in the rainy season. In December 1997, because the network setup and the data taking software were modified, operation became more stable than previously, and since then the observation has rarely been stopped.

The images are sometimes contaminated or covered by clouds. In order to avoid interference by the cloud pattern, two criteria have been used. First, if the motion of the pattern is too fast we do not use the images. This can be appropriately applied to our dataset because at Shigaraki, Japan, the westerly wind is prevailing almost all the time. Secondly, if the wave pattern changes the brightness of the stars, the images are recognized as a cloud pattern and are abandoned. Almost all the cloud contamination is easily found with the first criterion. However, the second is occasionally used when the tropospheric wind is weak in summer.

2.2 Analysis of the image data

Figure 3 shows an example of an image taken on 00:30:00–00:31:40 LT on December 28, 1997. The horizontal extent of the image at the OH altitude (∼87 km) is about 170 × 170 km in the NS and EW directions, whereas in the diagonal direction it is about 399 km. The bottom panel of Fig. 3 is a projection in the geographic coordinate. The images are often dominated by a wave-like structure, as shown in the figure, which is considered to be modulation of the airglow layer by the gravity waves. The horizontal wavelength and the direction of isophase lines are determined from the figure in the geographic coordinate, and the horizontal phase speed can be derived from several successive images. Thus, the horizontal wavelength and horizontal phase velocity (speed and direction) were determined from the image, and then the observed wave period is calculated. For the wave shown in Fig. 3 these parameters are determined to be 25 km (horizontal wavelength), 165 degrees (azimuth of propagation direction), and 9.4 m/s (horizontal phase speed), and the corresponding wave period is 44 min. In this study, we con-

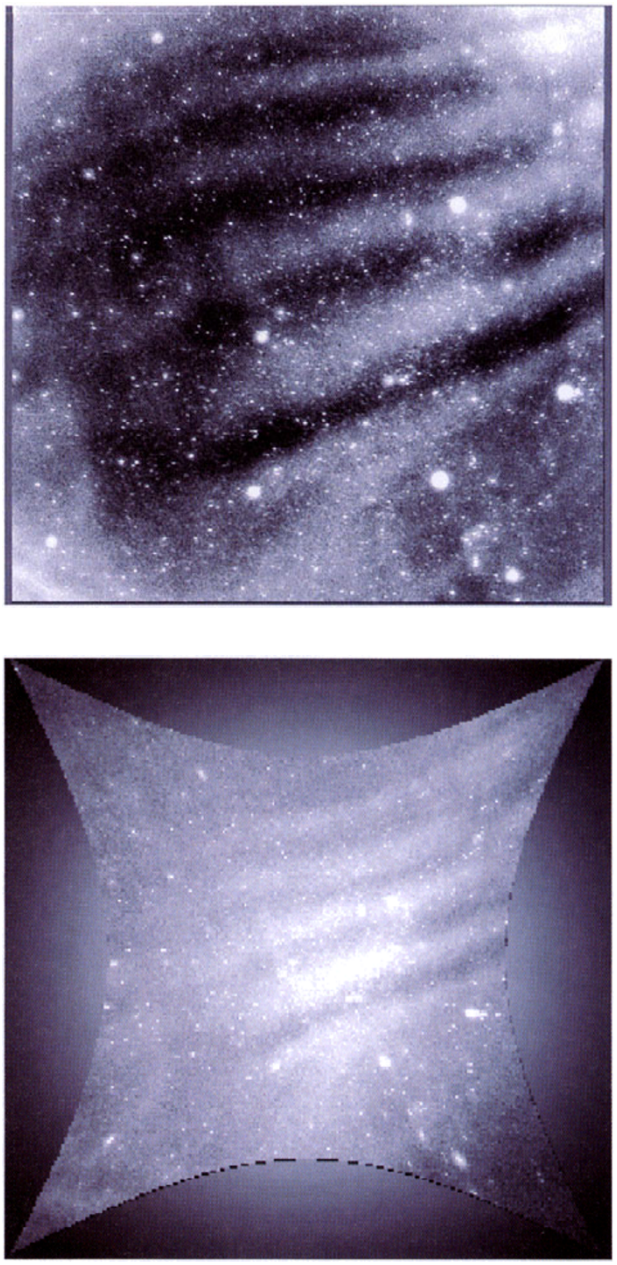

Fig. 3. An example of an OH airglow image taken at 00:30:00–00:31:40 on Dec 28, 1997. The top panel shows the raw image, and the bottom panel shows the transformation to the geographic coordinate assuming the OH airglow height is 87 km. The scale in the bottom panel is 256 km × 256 km. The upper and left sides correspond to the N and W directions, respectively.

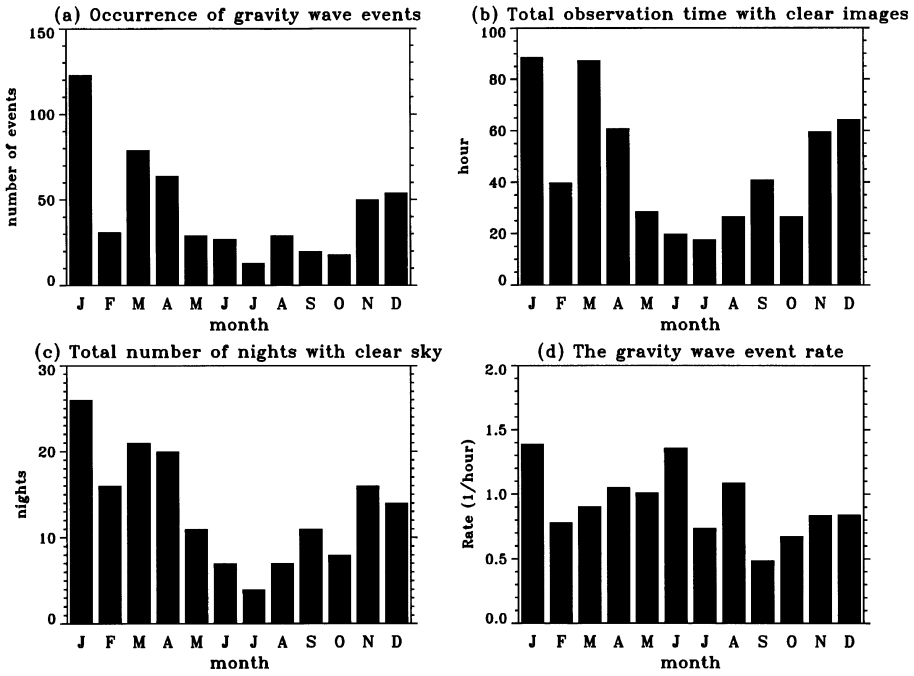

Fig. 4. Histograms of (a) the occurrence of gravity wave events, (b) the total observation time (hours) with clear images in a month, (c) the total number of nights with a clear sky, and (d) the gravity wave event rate per hour during the observation period from November 1996 to May 1998.

centrate on the dominant component of the gravity waves in the raw image data and pick the parameters of these gravity wave in order to study the characteristics of the gravity waves. In the previous studies involving airglow imagers (Peterson, 1979; Clairemidi *et al.*, 1985), these wave-like patterns were divided into "bands" and "ripples" according to the horizontal extent of the waves and the horizontal wavelengths (the former are large and extensive, and the latter are small and exist only in a limited area of the sky). However, the current images were obtained with a wide-view camera, and thus it is difficult to distinguish ripples and bands in the limited field of view. Therefore, we discuss the characteristics of the gravity waves according to the wavelengths, and do not classify the images into bands or ripples based on the horizontal extent.

3. Results

From 161 night observations with clear sky images, we have picked 536 wave events as dominant waves seen in the OH images. We have here defined that a gravity wave "event" is a wave-like pattern seen in OH images, which lasts at least for three successive images (i.e. for 9 minutes), the wave parameters not changing significantly. Note that most of the gravity wave events lasted less than one hour, although some events lasted for a few hours. The data for all the nights with at least a few images with a clear sky are included in the statistics of the event rate. Figure 4 shows the number of events observed each month. The total number of hours of clear sky was small in the summer and large in the winter, but this is partly because of the shorter nights in summer, and partly because the observations in winter and spring were carried out in two years. The average rate of gravity wave events was about 0.9/hour, with a slight seasonal variation, with a larger event rate in summer (except for July) and in winter (except for February), and less frequent events in equinoctial months. This is probably due to the more intensive activity of gravity waves in solstitial seasons in the MLT region (e.g., Tsuda *et al.*, 1994), but more accumulation of the data is necessary for a detailed discussion.

Figure 5 displays the distribution of the observed gravity wave parameters in each season. The whole observation period is separated into four seasons, November to February, March to April, May to August, and September to October, which correspond to winter, spring, summer, and autumn, respectively. In general, the horizontal wavelengths range from 5 km to 60 km, and the phase speed is distributed between 0 m/s and 100 m/s. The periods of the waves are between 5 and 30 min.

In spring and autumn, the major part of the horizontal wavelength distribution is around 15–35 km, and there are not many waves with horizontal wavelengths smaller than 15 km, i.e. small scale waves. However, in summer and winter, the major part of the waves is distributed between 5 and 35 km, with significant numbers below 15 km. Periods of between 5 and 10 minutes are more commonly seen in all seasons, however, in equinoctial months, periods of longer than 10 minutes are not frequent but are usually seen in winter and summer. Thus, the horizontal wavelengths and wave periods are distributed more widely in summer and winter, and less so in spring and autumn. The phase speeds in summer and winter are again similar, with distributions from 0 m/s to 80–100 m/s, with a peak at around 20–30 m/s. However, in spring and autumn, the waves with small phase speeds are not so frequent, and this tendency is more clearly seen in spring rather than in autumn. The major part of the waves in spring has phase speeds of 40–75 m/s.

The most remarkable seasonal variation is found in the hor-

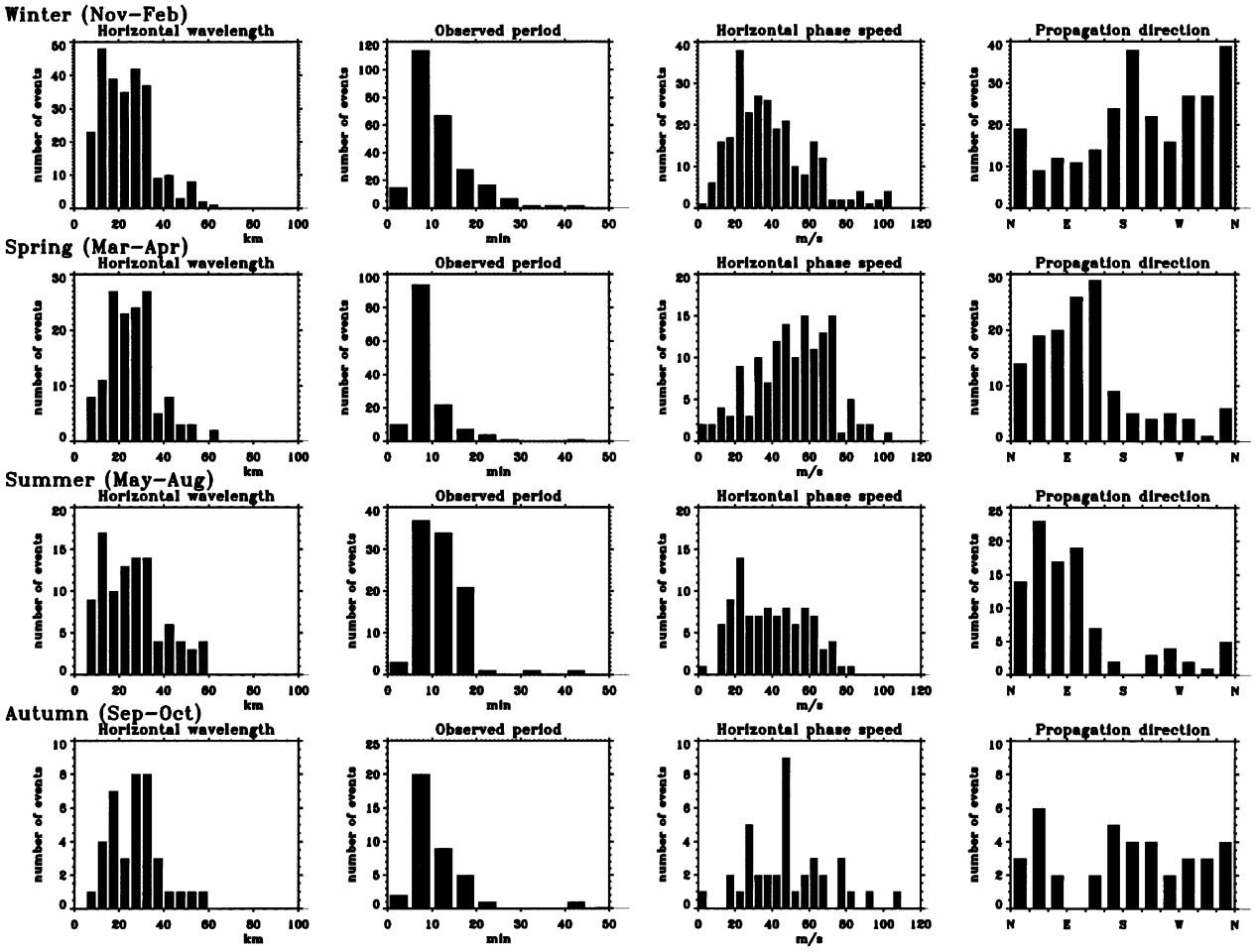

Fig. 5. Distribution of gravity wave parameters in each season. From the left, horizontal wavelengths, wave periods, phase speeds, and propagation directions are plotted. The top, 2nd, 3rd and bottom rows correspond to the winter, spring, summer, and autumn seasons (see text).

izontal propagation direction (or the direction of horizontal phase velocity). In summer, most waves propagated between northward and eastward. In winter, westward propagation is more common than eastward. The distribution in spring is similar to that in summer, but in autumn, the direction is more evenly distributed. Thus, the propagation direction of gravity waves is eastward in summer and spring, and westward in winter. This probably corresponds to the seasonal variation of the zonal wind in the middle atmosphere and reflects the filtering of gravity waves in the middle atmosphere. The details will be discussed in the following section.

Considering that there are not many waves with short horizontal wavelengths in equinoctial months, we here classify all the observed gravity waves into two groups, which are the groups of gravity waves with horizontal wavelengths of larger and smaller than 17.5 km, respectively (hereafter called L (large scale) and S (small scale), respectively). This wavelength of the boundary between the two groups corresponds to that "ripple type" and "band type" waves are reported to have the horizontal waves mainly smaller or larger than 17–18 km, as observed on airglow CCD imaging observation in Brazil by Taylor *et al.* (1997).

Figures 6, 7 and 8 show comparisons of the L type and S type waves in the distributions of the wave period, horizontal phase speed, and horizontal propagation direction, respectively, where histograms are plotted for the four seasons. The observed periods in Fig. 6 are generally small and large for small scale (S) and large scale (L) waves, respectively, although for both cases periods of between 5–10 minutes are frequently observed. For the waves, L, the wave periods are relatively small in spring and autumn (mainly between 5 and 10 minutes), whereas in summer and winter they become larger, exhibiting a wider distribution of between 5 and 25 minutes. The small scale waves (S) do not exhibit a clear seasonal variation. The horizontal phase speed in Fig. 7 showed in general larger and smaller values for the L and S components, respectively. The phase speeds of L waves are mainly between 20–80 m/s in summer and winter, but apparently larger in spring (major part exists between 40 and 80 m/s). The tendency of L waves in autumn is not clear because of the small sample number. The horizontal phase speed of the short scale (S) waves again does not exhibit clear seasonal variation.

As for the horizontal propagation direction shown in Fig. 8, the histograms of the L waves in spring, summer and autumn are very similar to those shown in Fig. 5 before the classification according to the horizontal waves, that is, eastward propagation in summer and spring, and no preferential direction

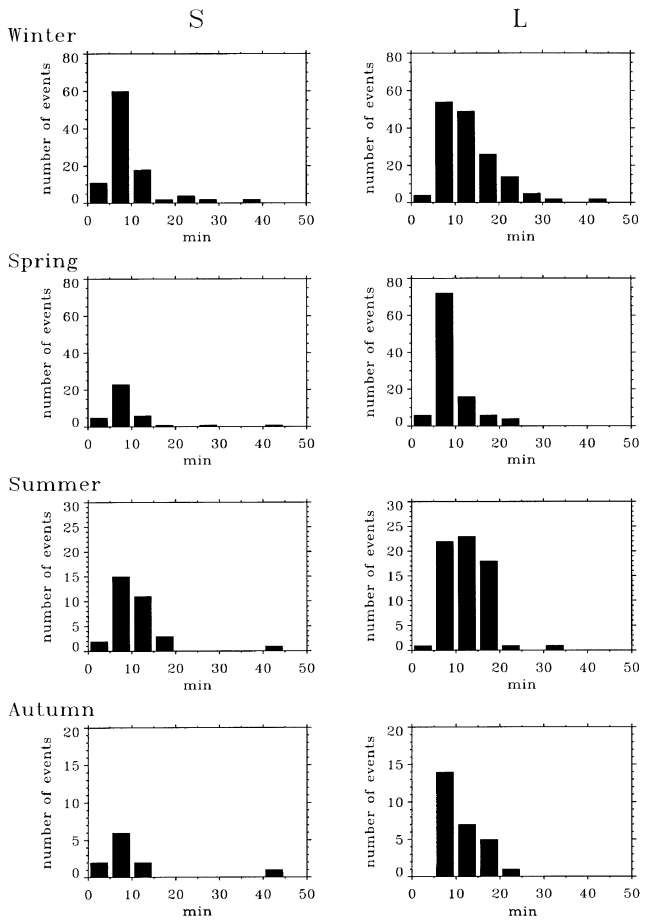

Fig. 6. Distribution of the wave period of the gravity waves for the horizontal wavelengths of less than 17.5 km (left), and larger than 17.5 km (right). The data for winter, spring, summer, and autumn are plotted from the top to the bottom.

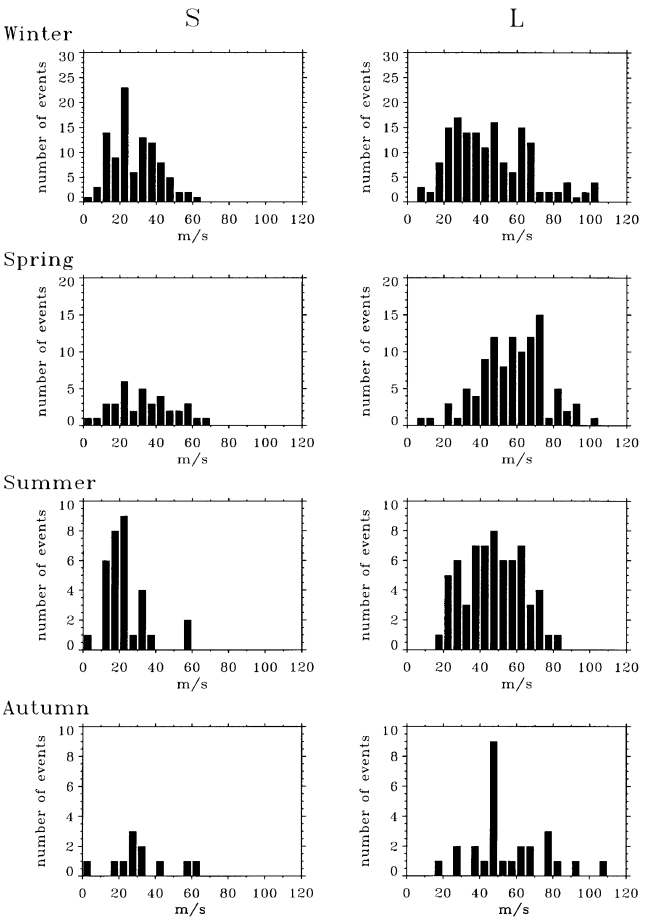

Fig. 7. Distribution of the horizontal phase speed of the gravity waves for horizontal wavelengths of less than 17.5 km (left), and larger than 17.5 km (right).

in autumn. However, in winter the distribution of L waves shows a more clear preference as to direction (westward) than that in Fig. 5 (L + S). On the contrary, the distribution of S waves shows a less clear preferential direction and is close to omnidirectional. Thus, the characteristics of the horizontal propagation direction are sensitive to the wave scale. It is noteworthy that small scale waves (S) in summer have a tendency to propagate between northward and south-eastward more preferentially, and in autumn in SE to W directions, respectively, although the latter is less clear due to the small event number. Thus, the small scale waves are more likely to propagate in wide directions, but also exhibit trends in summer and autumn.

In order to demonstrate the seasonal variation of the propagation direction more clearly, the distribution of each gravity wave event is plotted as scatter diagrams as to the day of the year and the propagation direction (azimuth) in Fig. 9. From the top panel of Fig. 9 it can be clearly seen that for the large scale (L) gravity waves in our study the preference of eastward propagation in summer lasts from March to September and the winter westward direction continues from October to the middle of March. The transitions between the summer state and the winter state is considered to be at the beginning to the middle of March and at the end of September. It is also notable that the wave propagation direction in mid-summer, i.e., from June to August, is likely to shift to northward from eastward, and this is more strongly observed in July. As for the shorter scale waves (S) shown in the bottom panel of Fig. 9, the preferential direction is much less clear than that of L waves, as was discussed above. However, the tendency of a N to SE direction in spring and summer (April to July) can be more clearly seen than in Fig. 8. It is notable that in August and September, L waves propagate mainly in azimuths between N and SE, but S waves exhibited less clear tendency compared with in April–July. Thus, the preferential direction seen in summer (eastward) continues longer for the L component waves, only lasting until July for the S component waves.

4. Discussion

The previous measurement of short period (<1 hour) gravity waves in the airglow layer by means of imagers revealed that there are waves with various horizontal wavelengths between 5 and 100 km (Clairemidi *et al.*, 1985; Armstrong, 1986). They are classified into two types; bands and ripples. The bands are extensive and long lasting wave patterns with horizontal wavelengths of several tens of km (Clairemidi *et al.*, 1985). Whereas, the ripples have wavelengths of ~5–15 km and are short-lived (<45 min) with a restricted spatial

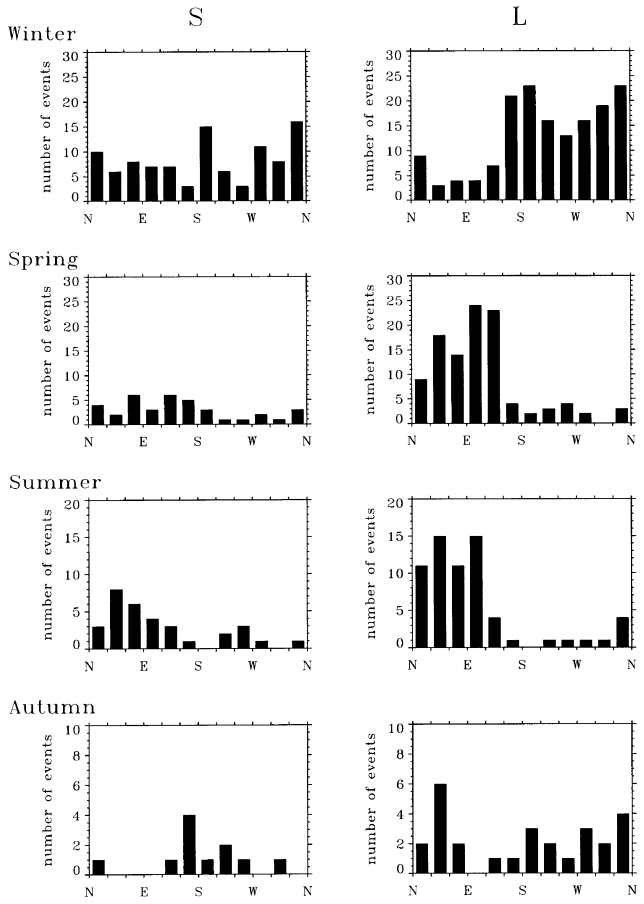

Fig. 8. Distribution of the horizontal propagation direction of the gravity waves for horizontal wavelengths of less than 17.5 km (left), and larger than 17.5 km (right).

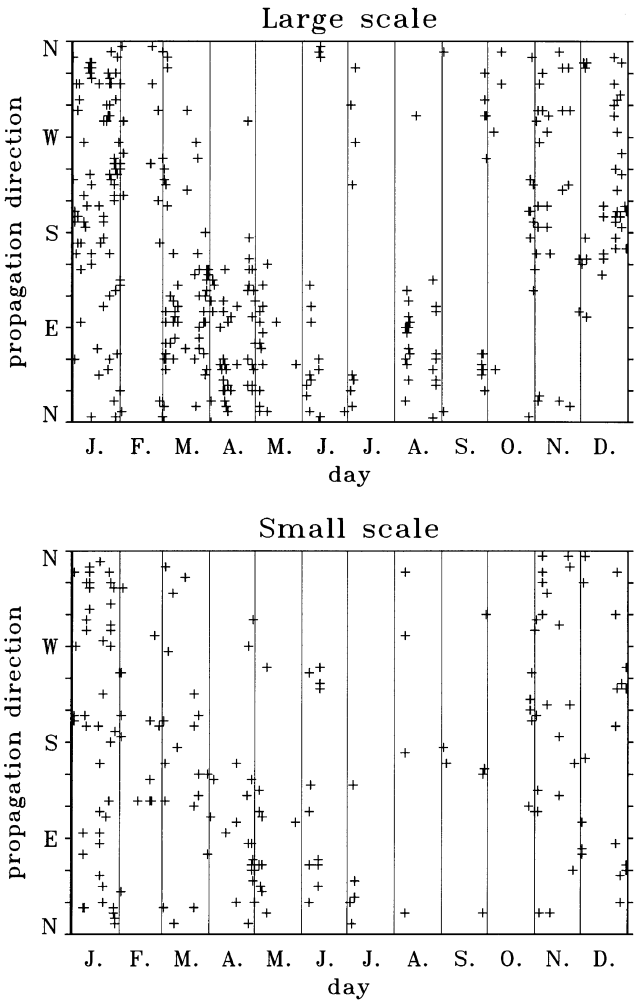

Fig. 9. Distribution of the horizontal propagation directions as a function of the month in a year. The top and bottom panels correspond to the waves with horizontal wavelengths of larger and smaller than 17.5 km, respectively.

extent (Peterson, 1979). The origin of the former waves is thought to be gravity waves propagated from the lower atmosphere (Taylor *et al.*, 1987), but the latter ones are considered to be generated *in-situ* through shear instability (Taylor and Hapgood, 1990), or through convective instability (Fritts *et al.*, 1993).

Bands are more commonly observed and reported on airglow imaging, however, ripples are not well reported because of their transient short-lived feature (Taylor *et al.*, 1997). Recent extensive observations (Taylor *et al.*, 1995, 1997) involved investigation of the ripple and band structure with multicolor allsky images of the airglow layer, and the difference of the origin has been discussed. On the other hand, a case study of the small scale wave structure (with horizontal wavelengths of 5–10 km) has been carried out with simultaneous imager, lidar and radar observations (Hecht *et al.*, 1997), and by numerical modeling in a companion paper (Fritts *et al.*, 1997). They found that convective instability induced by a larger scale gravity wave is the source of such a small scale wave-like pattern. In this study, we tried to follow the criteria of ripples and bands to our whole wave events, but classified them merely according to the horizontal wavelengths in the OH images because of the limited FOV. We first discuss the relation between the criteria of large scale (L) and small scale (S) waves in this study, and then that of "ripples and bands". Taylor *et al.* (1997) reported, based on two months observation in Brazil in equinoctial months, that ripples and bands have horizontal wavelengths of 6–18 km and 14–42 km, respectively. In this study, we defined the boundary as 17.5 km, and divided the whole events into band-like (L) and ripple-like (S) structures, although this border line is not perfect for separating these events, exclusively. Most of the waves with small scale (S) had periods of shorter than 10 minutes, which agrees well with the finding of Taylor *et al.* (1997). The horizontal phase speeds of S and L waves were 10–60 m/s and 10–100 m/s, respectively, with smaller phase speeds for smaller waves, which is very similar to the finding of Taylor *et al.* (1997). The distribution of azimuth angles for short waves is much wider than that of large scale waves, which again is similar to the report by Taylor *et al.* (1997). Thus, it is very likely that the waves with horizontal wavelengths larger and smaller than 17.5 km indicated by L and S in this study are mostly band type waves and ripple waves, respectively.

The horizontal propagation direction of the larger scale waves (L: $\lambda_h > 17.5$ km) observed in this study showed

clear seasonal variation with a direction preference of eastward/westward in the summer/winter seasons, with a transition at the beginning to the middle of March and the end of September. In mid-summer the preferential direction shifts from eastward to northward. These characteristics are very similar to those of mesospheric gravity waves (at around 70–80 km) observed with the MU radar. These waves observed with the MU radar have longer periods (5–15 hours) and larger horizontal wavelengths (500–1500 km) (Nakamura *et al.*, 1993b). Almost all the gravity waves shown by Nakamura *et al.* showed upward group velocity, and these waves are thought to be propagated upward in the middle atmosphere and affected by the filtering effect of the middle atmosphere jet. Similarly, the momentum flux due to shorter period gravity waves (5 min–2 hours) observed with the MU radar also indicated that eastward and westward propagating gravity waves are dominant in summer and winter, respectively (Tsuda *et al.*, 1990), which again is similar to the results obtained in this study for L scale gravity waves. On the other hand, the gravity waves of shorter scale (S) observed in this study showed much less significant seasonal variation of the horizontal propagation direction, as well as the period and horizontal phase speed.

It is considered that the gravity waves with a horizontal scale of larger than 17.5 km observed in this study (L) are generated in the lower atmosphere, possibly in the troposphere because of distinct seasonal variation of the propagation direction of eastward/westward in summer/winter, which is consistent with the filtering theory of gravity waves in the middle atmosphere (Lindzen, 1981). Taylor *et al.* (1993) suggested, on the basis of observations in summer months of May–July in Colorado (40°N), that the preferential direction of the gravity waves seen in the OH airglow is due to the filtering by the middle atmosphere wind. In our study, we used more than one year observations and showed the filtering effect of these waves more clearly. On the contrary, the gravity waves with a horizontal scale of smaller than 17.5 km observed in this study (S) are not filtered by the middle atmospheric wind, since they do not show clear seasonal variation. It is probable that these waves are generated above the middle atmospheric jet existing at around 50–70 km altitude. This is consistent with the suggestions by previous workers that these small scale waves are locally generated near the mesopause region through shear instability (Taylor and Hapgood, 1990) or convective instability (Fritts *et al.*, 1993, 1997). However, it is notable that, as shown in summer months, these small scale waves sometimes show a preferential propagation direction, and therefore a part of these waves can be generated in the lower atmosphere. One explanation is that the boundary of 17.5 km used to distinguish S and L waves is too large as a physical boundary in order to separate vertically propagating and *in-situ* waves. Another explanation for the remaining preferential direction for the small scale waves is that even in the case of *in-situ* generated instability, there could be a correlation of the directions between the larger scale waves and wave-like pattern due to instability (Fritts *et al.*, 1997; Hecht *et al.*, 1997), and hence it is possible to have a non-uniform azimuthal distribution and its seasonal variation. In order to clarify these possibilities it would be worthwhile obtaining more statistics with smaller wavelengths as the boundary. However, this is not easy from our current database because of insufficient samples of waves with small horizontal wavelengths such as <10 km. Observations with shorter time intervals of images are necessary to discuss further statistics of such small scale waves.

The differences in the gravity wave parameters, such as horizontal wavelengths, periods and phase speeds, between summer/winter months and equinoctial months are also an interesting finding in this study. One possible explanation is that the waves with a slow horizontal phase speed (which are likely to have longer periods and shorter horizontal wavelengths) could not propagate upward in the middle atmosphere under a weak wind condition in equinoctial months, and therefore the observed waves in the equinoctial seasons are of short period, long horizontal wavelength and fast horizontal phase velocity.

On the other hand, the lack of waves of small scale and slow phase speed could also be explained by the seasonal variation of the occurrence of the generation of small scale waves near the mesopause due to instability, which can be modified by the activity of atmospheric waves such as larger scale gravity waves. The semiannual variation of the gravity wave activity in the mesosphere revealed by many radar studies (e.g., Tsuda *et al.*, 1994) agrees with this scenario.

At the moment we do not have a clear answer regarding the alternatives discussed above, but detailed analysis of the background wind field using the MU radar data in future will be helpful in explaining the existing differences between summer/winter and equinoctial months.

5. Conclusion

OH airglow imager observations have been carried out at Shigaraki, Japan (35°N, 136°E), since November 1996. In this paper the observations in first 18 months are analyzed, in order to pick up the dominant gravity wave pattern in the OH images. The time and spatial scales of these waves are typically 5–30 minutes (observed period) and 5–60 km (horizontal wavelength), respectively. Wave parameters such as horizontal wavelength, period, and horizontal phase velocities (speed and direction) are investigated for four seasons, i.e. summer (May–Aug), winter (Nov–Feb), spring (Mar–Apr), and autumn (Sep–Oct). The distributions of the horizontal wave length, wave period and horizontal phase speed are different between summer/winter and the equinoxes. In equinoctial months, small scale waves (<15 km), long period waves (>10 min), and slow waves (phase speed <30 m/s) are significantly less frequent than in summer/winter. The horizontal propagation direction (direction of phase velocity) showed clear seasonal variations with an eastward/westward preference in summer/winter, respectively, with a transition in the middle of March and the end of September, which corresponds well with the wave filtering by the middle atmosphere wind. However, the small scale gravity waves with wavelengths of less than 17.5 km (this scale is similar to that of "ripples") which have short periods (around 5–10 min) and slow phase speeds (<40 m/s) do not show a clear change of the propagation direction, but the distribution is close to omni-directional with some preferential direction.

Thus, the gravity waves observed in the OH layer ($\sim$87

km altitude) with horizontal wavelengths of larger than 18 km are considered to be generated in the troposphere and propagated through the middle atmosphere, which is similar to the gravity waves of a larger scale observed with the MU radar in the mesosphere (Nakamura *et al.*, 1993b). However, the origin of the small scale waves (horizontal wavelengths <17 km) is mainly *in-situ* generation in the mesosphere with possible mixing with waves from the troposphere. One possibility for the mixture is that the physical boundary between the waves of tropospheric origin and *in-situ* generation could be smaller than 17 km, as used in this study, as suggested by Hecht *et al.* (1997).

Acknowledgments. The authors are grateful to Prof. Hiroshi Fukunishi, Dr. Yukihiro Takahashi, and Mr. Yoshinoli Yamada of Tohoku University, and Prof. Shoichi Okano of National Institute of Polar Research for their help and suggestions regarding development of the CCD imager. The MU radar belongs to and is operated by Radio Atmospheric Science Center, Kyoto University.

References

Armstrong, E. B., Irregularities in the 80–100 km region: A photographic approach, *Radio Sci.*, **21**, 313, 1986.

Clairemidi, J., M. Herse, and G. Moreels, Bi-dimensional observation of waves near the mesopause at auroral latitudes, *Planet. Space Sci.*, **33**, 1013–1022, 1985.

Fritts, D. C., J. R. Isler, G. Thomas, and Ø. Andreassen, Wave breaking signatures in noctilucent clouds, *Geophys. Res. Lett.*, **20**, 2039–2042, 1993.

Fritts, D. C., J. R. Isler, J. H. Hecht, R. L. Walterscheid, and Ø. Andreassen, Wave breaking signature in sodium densities and OH nightglow, 2. Simulation of wave and instability structure, *J. Geophys. Res.*, **102**, 6669–6684, 1997.

Gardner, C. S. and M. J. Taylor, Observational limits for lidar, radar, and airglow imager measurements of gravity wave parameters, *J. Geophys. Res.*, **103**, 6427–6437, 1998.

Hecht, J. H., R. L. Walterscheid, D. C. Fritts, J. R. Isler, D. C. Senft, C. S. Gardner, and S. J. Franke, Wave breaking signature in OH airglow and sodium densities and temperatures 1. Airglow imaging, Na lidar, and MF radar observations, *J. Geophys. Res.*, **102**, 6655–6668, 1997.

Isler, J. R., M. J. Taylor, and D. C. Fritts, Observational evidence of wave ducting and evanescence in the mesosphere, *J. Geophys. Res.*, **102**, 26301–26313, 1997.

Lindzen, R. S., Turbulence and stress owing to gravity wave and tidal breakdown, *J. Geophys. Res.*, **86**, 9707–9714, 1981.

Manson, A. H. and C. E. Meek, Gravity wave propagation characteristics (60–120 km) as determined by the Saskatoon MF Radar (GRAVNET) system: 1983–85 at 52°N, 107°W, *J. Atmos. Sci.*, **45**, 932–946, 1988.

Nakamura, T., T. Tsuda, M. Yamamoto, S. Fukao, and S. Kato, Characteristics of gravity waves in the mesosphere observed with the MU radar, 1. Momentum flux, *J. Geophys. Res.*, **98**, 8899–8910, 1993a.

Nakamura, T., T. Tsuda, M. Yamamoto, S. Fukao, and S. Kato, Characteristics of gravity waves in the mesosphere observed with the MU radar, 2. Propagation direction, *J. Geophys. Res.*, **98**, 8911–8923, 1993b.

Peterson, A. W., Airglow events visible to the naked eye, *App. Opt.*, **18**, 3390, 1979.

Shiokawa, K., Y. Katoh, M. Satoh, M. K. Ejiri, T. Ogawa, T. Nakamura, T. Tsuda, and R. H. Wiens, Development of Optical Mesosphere Thermosphere Imagers (OMTI), *Earth Planets Space*, **51**, this issue, 887–896, 1999.

Taylor, M. J. and M. A. Hapgood, Identification of a thunderstorm as a source of short period gravity waves in the upper atmospheric nightglow emission, *Planet. Space Sci.*, **36**, 975–985, 1988.

Taylor, M. J. and M. A. Hapgood, On the origin of ripple-type wave structure in the OH nightglow emission, *Planet. Space Sci.*, **38**, 1421–1430, 1990.

Taylor, M. J., M. A. Hapgood, and P. Rothwell, Observations of gravity wave propagation in the OI (5577 nm), Na (589.2 nm) and the near infrared OH nightglow emissions, *Planet. Space Sci.*, **35**, 413–427, 1987.

Taylor, M. J., E. H. Ryan, T. F. Tuan, and R. Edwards, Evidence of preferential directions for gravity wave propagation due to wind filtering in the middle atmosphere, *J. Geophys. Res.*, **98**, 6047–6057, 1993.

Taylor, M. J., M. B. Bishop, and V. Taylor, All-sky measurements of short period waves imaged in the OI (557.7 nm), Na (589.2 nm) and near infrared OH and O_2 (0, 1) nightglow emissions during the ALOHA-93 campaign, *Geophys. Res. Lett.*, **22**, 2833–2836, 1995.

Taylor, M. J., W. R. Pendleton, Jr., S. Clark, H. Takahashi, D. Gobbi, and R. A. Goldberg, Image measurements of short period gravity waves at equatorial latitudes, *J. Geophys. Res.*, **102**, 26283–26299, 1997.

Tsuda, T., Y. Murayama, M. Yamamoto, S. Kato, and S. Fukao, Seasonal variation of momentum flux in the mesosphere observed with the MU radar, *Geophys. Res. Lett.*, **17**, 725–728, 1990.

Tsuda, T., Y. Murayama, T. Nakamura, R. A. Vincent, A. H. Manson, C. E. Meek, and R. L. Wilson, Variations of the Gravity Wave Characteristics with Height, Season and Latitude Revealed by Comparative Observations, *J. Atmos. Terr. Phys.*, **56**, 555–568, 1994.

Wu, Q. and T. L. Killeen, Seasonal Dependence of Mesospheric Gravity Waves (<100 km) at Peach Mountain Observatory, Michigan, *Geophys. Res. Lett.*, **23**, 2211–2214, 1996.

T. Nakamura (e-mail: nakamura@kurasc.kyoto-u.ac.jp), A. Higashikawa, T. Tsuda, and Y. Matsushita